第36卷 第1期 焊 接 学 报 Vol. 36 No. 1
2015年1月 TRANSACTIONS OF THE CHINA WELDING INSTITUTION January 2015

搅拌头旋转频率对静止轴肩搅拌摩擦焊接头力学性能的影响规律

姬书得[1,2]， 孟祥晨[1]， 黄永宪[2]， 高双胜[1]， 路 浩[3]， 马 琳[1]

(1. 沈阳航空航天大学 航空航天工程学部，沈阳 110136;
2. 哈尔滨工业大学 先进焊接与连接国家重点实验室，哈尔滨 150001;
3. 南车青岛四方机车车辆股份有限公司，青岛 266111)

摘 要: 利用自行设计的静止轴肩装置对6005A-T6铝合金进行了静止轴肩搅拌摩擦焊的试验研究. 结果表明，当焊接速度为200 mm/min时，表面光滑且无缺陷的焊接接头抗拉强度与断后伸长率随着搅拌头旋转频率的增加呈现先增加后减小的趋势; 焊接接头的正背弯180°无裂纹; 当旋转频率为1 800 r/min时，抗拉强度达到最大值234 MPa，接头强度系数达到79%. 静止轴肩搅拌摩擦焊接头的显微维氏硬度呈W形分布，最小值出现在前进侧的热影响区; 接头的软化程度随搅拌头旋转频率的增加而增加. 焊接接头的断裂位置位于热力影响区，断口呈韧性断裂.

关键词: 静止轴肩搅拌摩擦焊; 力学性能; 搅拌头旋转频率; 断口

中图分类号: TG 453 **文献标识码**: A **文章编号**: 0253-360X(2015)01-0051-04

0 序 言

作为固相连接技术，搅拌摩擦焊(friction stir welding，FSW)具有接头质量高、能耗低、绿色无污染等优点，目前广泛应用于航空、航天、交通等领域[1-3]. 事实上在常规的FSW过程中，搅拌头需高速旋转并向焊板施加非常大的垂向作用力以保证足够的热输入; 焊缝表面的弧纹随着搅拌头在焊接过程中前进而产生，这也是常规FSW接头的典型宏观特征[4]. 表面弧纹的存在不利于接头的性能与表面光滑性，而静止轴肩搅拌摩擦焊(stationary shoulder friction stir welding，SSFSW)可有效地消除表面弧纹[5].

目前国内外的研究者对SSFSW的对接、角接等接头性能进行了研究[5-10]. Li等人[6]获得了无缺陷的AA2219-T6铝合金SSFSW的对接接头. 吉华等人[7]以6061-T6铝合金为研究对象，获得了达到母材抗拉强度65%以上SSFSW的T形接头. Wynne与Daries等人[8,9]的研究结果表明，SSFSW焊接钛合金时可有效避免沿焊缝厚度方向组织不均匀的情况. 尽管目前有关SSFSW的研究取得了一些成果，但技术积累明显不足，使SSFSW的实际工程应用存在较大困难. 文中以6005A-T6铝合金为研究对象，分析了SSFSW的焊缝成形以及力学性能，研究了旋转频率对接头抗拉强度、断口形貌等的影响.

收稿日期: 2014-03-17
基金项目: 国家自然科学基金资助项目(51204111); 航空科学基金资助项目(2013ZE54021，2014ZE54021); 先进焊接与连接国家重点实验室基金资助项目(AWJ-M13-07)

1 试验方法

以6005A-T6铝合金材料为研究对象进行SSFSW的对接试验. 试板尺寸为500 mm×150 mm×4.0 mm. 6005A-T6铝合金的抗拉强度为298 MPa，断后伸长率为9.7%.

对焊缝区域的材料表面进行打磨后，在型号为FSW-3LM-4012的搅拌摩擦焊设备上进行SSFSW试验. SSFSW的焊接装置主要由外部的不旋转的静轴肩体与内部的可旋转的搅拌头等组成. 在焊接过程中，外部的静轴肩与内部的搅拌头同步沿焊接方向移动并实现焊接. 文中使用的焊接装置如图1所示. 静轴肩的内径与外径分别为6.3与14 mm; 搅拌头由小轴肩与带螺纹的搅拌针组成，小轴肩的直径为6 mm，搅拌针的根部直径与尖端直径分别为4与3 mm.

文中采用的搅拌头旋转频率分别为1 600，1 700，1 800，1 900与2 000 r/min，焊接速度为200 mm/min. 焊后的SSFSW接头的拉伸与弯曲试验均在型号为RG4300的电子万能试验机上进行测试，拉伸速度为1 mm/min; 断口利用型号为KYKY-

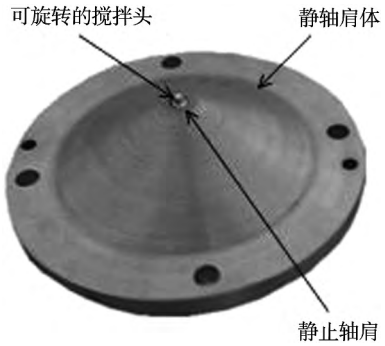

图 1 焊接用静止轴肩装置

Fig. 1 Stationary shoulder equipment used in experiment

2800B 的扫描电子显微镜分析.

2 试验结果与讨论

与常规搅拌摩擦焊类似,在静止轴肩搅拌摩擦焊过程中可旋转的搅拌头亦产生表面弧纹; 在焊接过程中,搅拌头外部静止轴肩会对表面弧纹产生"抹"的作用,从而消除弧纹并获得表面光滑的 SSFSW 接头,如图 2 所示. 同时静止轴肩可有效地抑制高温下的塑性金属材料沿旋转的搅拌头轴肩两侧挤出,从而起到减少飞边尺寸的作用. 与常规 FSW 相比,SSFSW 接头飞边尺寸的减小相当于有更多的材料被挤入焊缝中,从而对于防止孔洞等缺陷的产生非常有利.

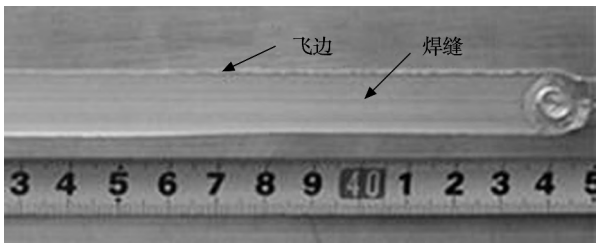

图 2 SSFSW 的焊接接头

Fig. 2 Welding joint of SSFSW

图 3 给出了典型焊接工艺参数(1 800 r/min, 200 mm/min) 下的拉伸与弯曲试验后的 SSFSW 接头形貌. 通过分析可知,SSFSW 接头的断裂位置位于热力影响区,且 SSFSW 接头的正背弯达到了 180°无裂纹. 与常规 FSW 类似[11],当焊接工艺不合理时,SSFSW 接头亦会出现根部未焊透、孔洞或隧道等缺陷,这些缺陷的存在会造成焊接接头在弯曲过程中断裂,使正弯或背弯试验的弯曲角难以达到 180°. 因此弯曲试验的结果也证明了焊缝中无未焊透或孔洞等缺陷的存在.

图 3 拉伸与弯曲后的 SSFSW 接头

Fig. 3 Welding joints of SSFSW after tensile experiment and bending experiment

图 4 是不同旋转频率下的 SSFSW 接头抗拉强度与断后伸长率的关系曲线. 通过分析可知,当焊接速度为 200 mm/min 时,SSFSW 接头的抗拉强度与断后伸长率均随搅拌头旋转频率的增加呈现先增加后减小的趋势; 当搅拌头旋转频率为 1 800 r/min 时,接头的抗拉强度与断后伸长率分别达到 234 MPa 与 6.1%,其值分别达到母材的 79% 与 63%.

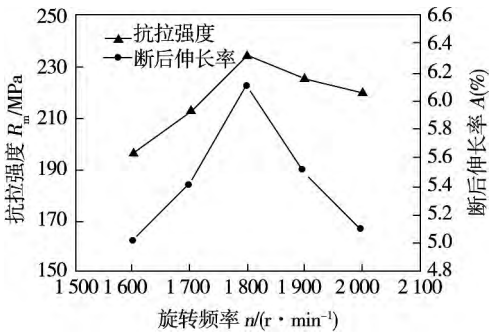

图 4 不同旋转频率下的抗拉强度与断后伸出长率

Fig. 4 Tensile strength and elongation under different rotational velocities

与常规 FSW 类似,在 SSFSW 过程中随着搅拌头旋转频率的增加,单位时间内的焊接热输入增加,造成焊接温度峰值的增加. 当焊接温度峰值较低时,材料的流动性较差,在焊接过程中材料可能无法有效填充搅拌头后方的空腔且材料受到的搅拌头搅拌混合的作用差,可能造成弱连接、孔洞甚至隧道等缺陷. 对于文中的 SSFSW 来说,静止轴肩在焊接过程中给予待焊板 0.2 mm 的压入量. 因此在焊接接头表面出现静止轴肩的存在引起的两道压痕,此压痕位于图 2 所示的飞边处. 事实上在焊后的拉伸试验过程中,压痕位置将产生由几何变化而导致的应力集中. 同时由于内部的旋转搅拌头的工作原理与常规 FSW 相同,因此在搅拌头作用区的边缘出现焊

接残余应力的峰值[12]. 几何应力集中、残余应力集中以及热力影响区或热影响区的软化现象共同作用,使 SSFSW 接头的断裂位置位于热力影响区(图 3). 相同的静轴肩装置造成的几何应力集中位置及大小几乎是不变的; 但当温度过高时,内部旋转搅拌头造成的焊接残余应力变大,不利于接头的性能. 因此从提高 SSFSW 接头抗拉强度的角度讲,焊接温度峰值过高或过低都是不利的,这也是 SSFSW 接头的抗拉强度随搅拌头旋转频率的增加呈现先增加后降低规律的原因.

图 5 是不同旋转频率下 SSFSW 接头的显微维氏硬度,其中各测试点位于沿焊缝厚度方向的中心. 通过分析可知,SSFSW 接头的显微维氏硬度在焊核中心线两侧基本上呈对称分布,从焊核到母材的硬度曲线呈 W 形分布,即焊核中心、热力影响区与热影响区等 3 个典型区域的显微维氏硬度均小于母材,且硬度最小值出现在热影响区; SSFSW 接头前进侧的硬度值略低于后退侧对应位置的硬度. 在 SSFSW 过程中,焊核区的金属材料不仅经历了最高温度下的热循环,还受到了非常大的应变以及应变速率,使材料发生了剧烈的动态再结晶,形成致密细小的等轴晶[13],因此硬度保持较高的数值; 热影响区的材料没有经历塑性变形,在焊接热的作用下出现晶粒长大现象,导致出现由粗大晶粒引起的硬度较低的现象. 就像前面叙述的那样,在 SSFSW 过程中,当焊接速度一定时,焊接温度峰值随着搅拌头旋转频率的增加而增加,且在沿垂直焊接方向上高温区域相应增加. 因此随着搅拌头旋转频率的增加,SSFSW 接头的软化程度增加且软化区域变宽. 由图 5 可知,当搅拌头旋转频率为 2 000 r/min 时,SSFSW 接头的硬度最小值为 61.7 HV,且软化区宽度约为 22 mm; 当搅拌头旋转频率为 1 600 r/min 时,SSFSW 接头的硬度最小值为 63.9 HV,且软化区宽度约为 18 mm.

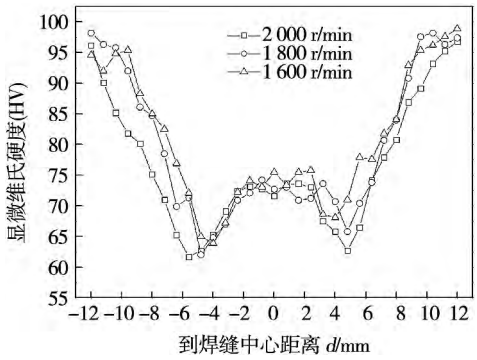

图 5　不同旋转频率下的 SSFSW 接头硬度

Fig. 5　Hardness of SSFSW joint under different rotational velocities

事实上对于图 3 所示的拉伸断口,焊件的断面有明显的分层,为典型的 45°塑性断裂外貌. 图 6 给出了不同旋转频率下的接头断口形貌,其中形貌特征取于焊件的中心. 通过分析可知,SSFSW 接头的断口由大量深浅不一的韧窝组成,为典型的韧性断裂. 结合图 4 中的断后伸长率曲线可知,在较大的断后伸长率,断口的韧窝大而深; 当焊接速度为 200 mm/min 且在搅拌头的旋转频率为 1 800 r/min,SSFSW 接头断口的韧窝最大且最深; 在搅拌头的旋转频率为 1 600 r/min 或 2 000 r/min,韧窝小而浅.

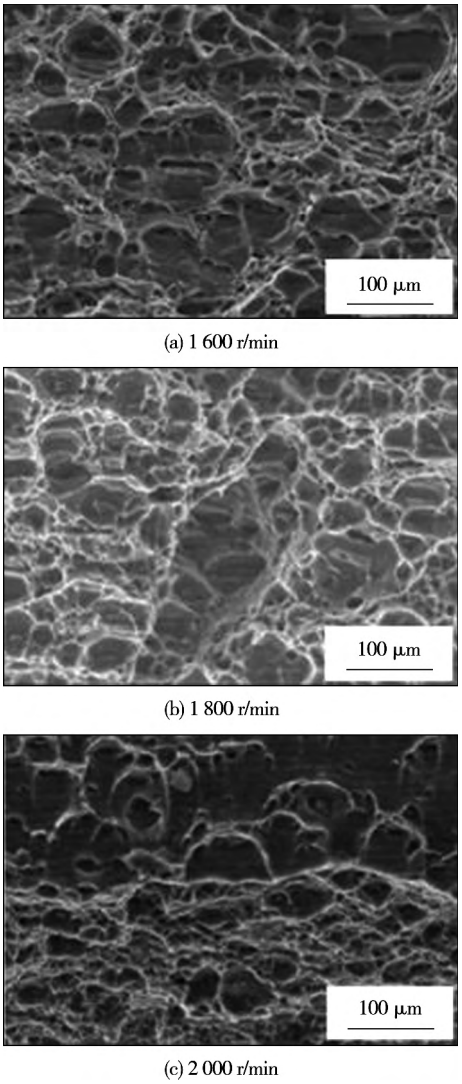

(a) 1 600 r/min

(b) 1 800 r/min

(c) 2 000 r/min

图 6　不同搅拌头旋转频率下的 SSFSW 断口形貌

Fig. 6　Fracture surface morphologies under different rotational velocities

3　结　　论

(1) 采用静止轴肩搅拌摩擦焊工艺对 6005A-T6 铝合金进行了对接试验,得到了焊件表面光滑、飞边小以及无未焊透缺陷的焊接接头.

(2) 当焊接速度一定时,随搅拌头旋转频率的增加,静止轴肩搅拌摩擦焊接头的抗拉强度与断后伸长率均呈现先增加后减少的趋势; 接头正背弯180°无裂纹. 当焊接速度为200 mm/min,搅拌头旋转频率为1 800 r/min时,接头的抗拉强度与断后伸长率分别达到234 MPa与6.1%,分别占母材79%与63%.

(3) 静止轴肩搅拌摩擦焊接头典型区域的硬度从大到小排列依次是母材、焊核、热力影响区、热影响区; 随旋转频率的增加,接头的软化程度与软化区宽度增加. 焊接接头的断裂位置是热力影响区; 断口由大量深浅不一的韧窝组成,是韧性断裂.

参考文献:

[1] Schmidt H B, Hattel J H. Thermalmodeling of friction stir welding [J]. Scirpta Materialia, 2008, 58(5): 332 - 337.

[2] 姬书得, 孟庆国, 史清宇, 等. 搅拌针形状影响搅拌摩擦焊过程金属塑性流动规律的数值模拟 [J]. 焊接学报, 2013, 34(2): 93 - 96.
Ji Shude, Meng Qingguo, Shi Qingyu, *et al*. Numerical simulation of metal plastic flow in friction stir welding affected by pin shape [J]. Transactions of the China Welding Institution, 2013, 34(2): 93 - 96.

[3] Wan L, Huang Y X, Lü Z L, *et al*. Effect of self-support friction stir welding on microstructure and microhardness of 6082-T6 aluminum alloy joint [J]. Materials and Design, 2014, 55: 197 - 203.

[4] 王大勇, 冯吉才. 搅拌摩擦焊焊缝表面弧形纹形成模型 [J]. 焊接学报, 2003, 24(5): 42 - 45.
Wang Dayong, Feng Jicai. Process model of arc corrugation on friction-stir weld [J]. Transactions of the China Welding Institution, 2003, 24(5): 42 - 45.

[5] 刘会杰, 李金全, 段卫军. 静止轴肩搅拌摩擦焊的研究进展 [J]. 焊接学报, 2012, 33(5): 108 - 112.
Liu Huijie, Li Jinquan, Duan Weijun. Progress in the stationary shoulder friction stirwelding [J]. Transactions of the China Welding Institution, 2012, 33(5): 108 - 112.

[6] Li J Q, Liu H J. Effects of tool rotation speed on microstructures and mechanical properties of AA2219-T6 welded by the external non-rotational shoulder assisted friction stir welding [J]. Materials and Design, 2013, 43: 299 - 306.

[7] 吉 华, 徐 萌, 封小松, 等. 静止轴肩搅拌摩擦焊T型接头组织及力学行为 [J]. 电焊机, 2013, 43(9): 37 - 40.
Ji Hua, Xu Meng, Feng Xiaosong, *et al*. Research on microstructure and mechanical behavior of T-joint welded by stationary shoulder friction stir welding [J]. Electric Welding Machine, 2013, 43(9): 37 - 40.

[8] Wynne B P, Threadgill P L, Davies P S, *et al*. Microstructure and texture in static shoulder friction stir welds of Ti-6Al-4V [C] // 7th International Friction Stir Welding Symposium, Awaji Island, Japan, 2008: 20 - 22.

[9] Davies P S, Wynne B P, Rainforth W M, *et al*. Development of microstructure and crystallographic texture during stationary shoulder friction stir welding of Ti-6Al-4V [J]. Metallurgical and Materials Transaction A, 2011, 42(8): 2278 - 2289.

[10] Ahmed M M Z, Wynne B P, Rainforth W M, *et al*. Through-thickness crystallographic texture of stationary shoulder friction stir welded aluminum [J]. Scripta Materialia, 2011, 64: 45 - 48.

[11] Chen H B, Yan K, Lin T, *et al*. The investigation of typical welding defects for 5456 aluminum alloy friction stir welds [J]. Materials Science and Engineering A, 2006, 433: 64 - 69.

[12] Javadi Y, Seyedali S, Najafabadi M A. Taguchi optimization and ultrasonic measurement of residual stresses in the friction stir welding [J]. Materials and Design, 2014, 55: 27 - 34.

[13] Etter A L, Baudin T, Fredj N, *et al*. Recrystallization mechanisms in 5251 H14 and 5251 O aluminum friction stir welds [J]. Materials Science and Engineering A, 2007, 445/446: 94 - 99.

作者简介: 姬书得,男,1977年出生,博士,副教授. 主要从事摩擦焊机理、工艺与仿真方面的研究工作. 发表论文30余篇. Email: superjsd@163.com

from nozzle to workpiece surface on cutting quality, 2 – 4 mm was employed in this study. As the cutting speed increased, the *reduction of laser cut width in the bottom was most obvious* and cleavage lines of laser cut became curved. When the speed reached to 2.0 *m/min*, *fracture surface of laser cut steel* was observed to be strip-like type.

Key words: *laser cutting*; *underwater cutting*; *underwater laser cutting*; 30 mm steel plate

Microstructure, bonding mechanism and corrosion property of titanium TA2/copper T2 welded joint by cold metal transfer technology CAO Rui, FENG Zhen, CHEN Jianhong, JING Min (State Key Laboratory of Advanced Processing and Recycling of Non-ferrous Metals, Lanzhou University of Technology, Lanzhou 730050, China). pp 39 – 42

Abstract: This paper described a fundamental investigation of titanium TA2-copper T2 butt joint by cold metal transfer (CMT). During the welding process, wire was deviated from the edge of Cu sheet. A satisfied Ti-Cu CMT welding-brazing butt joint was obtained. Fusion welding joint was formed at copper side, while brazing joint was formed at titanium side. Welding-brazing joint was formed between titanium TA2-copper T2. Bonding mechanism of the welded joints was examined by scanning electron microscopy (SEM) with energy dispersive spectrometer (EDS) and tensile tests. Corrosion tests of Ti/Cu welded joint were conducted in solution of 10% HCl at room temperature. Results indicated that brazing interface consisted of various intermetallic compounds, i. e. Ti_2Cu, TiCu, and $AlCu_2Ti$. And the weld metal was composed of α-Cu solid solution and Ti-Cu-Al-Ni-Fe multi-phase. The tensile strength of the joint can reach to 205 MPa. There were corrosion grooves in brazing interfaces after corrosion for 7 days, and self-fracture after corrosion for 14 days.

Key words: Ti/Cu dissimilar metals; cold metal transfer; bonding mechanism; corrosion property

Study on butt fusion welding characteristics of AZ31B magnesium alloy to steel by hybrid laser-TIG welding with Ni interlayer SONG Gang[1], HU Guanglong[1], REN Daxin[2], LIU Liming[1] (1. Key Laboratory of Liaoning Advanced Welding and Joining Technology, School of Materials Science and Engineering, Dalian University of Technology, Dalian 116024, China; 2. Key Laboratory of Materials Modification by Laser, Ion, and Electron Beams (Ministry of Education), School of Materials Science and Engineering, Dalian University of Technology, Dalian 116024, China). pp 43 – 46

Abstract: Investigations on butt fusion welding characteristics of AZ31B magnesium alloy to steel with Ni interlayer were carried out by utilizing the gradient energy density characteristic of laser-TIG heat source. The tensile strength and microstructure of the joint were examined by electronic tension machine, scanning electron microscopy (SEM) and X-ray diffraction (XRD). Results indicated that magnesium alloy can be butt joined to steel by hybrid laser-TIG welding with good Mg/Fe interface by using Ni foil as the interlayer. At the same time, tests showed that a distinct transition zone consisting of Fe, Ni and Al elements forms at the steel side nearby the interface; the microstructure of the joint is mainly composed of α-Mg and a large number of small white particles which are mainly composed of AlNi phase and dispersively distributed. The joint fractures nearby the Mg/Fe interface and the fracture surface shows a typical quasi-cleavage crack. The average of the joint tensile strength is 232 MPa, *which is about 90% of the magnesium base metal.*

Key words: hybrid laser-TIG heat source; butt joint; *magnesium alloy*; steel; *Ni interlayer*

Characteristics and mechanical properties of bypass-current MIG welding-brazed dissimilar Al/Ti joints MIAO Yugang[1], WANG Teng[1], ZHOU Yue[2], HAN Duanfeng[1] (1. National Key Laboratory of Science and Technology on Underwater Vehicle, *Harbin Engineering University*, *Harbin 150001*, China; 2. State Key Laboratory of Advanced Welding and Joining, *Harbin Institute of Technology*, *Harbin 150001*, *China*). pp 47 – 50

Abstract: *Joining of 1 mm thick aluminum 6061 to titanium TC4 was conducted by using bypass-current MIG welding-brazed*, and stable welding process and good bead appearance were obtained. The joint profile and microstructure of Ti/Al joints were observed by optical microscopy and SEM, and then the structure of the interfacial reaction layers were analyzed in details. It was found the intermetallic compound layer at the interfacial top is in the form of columnar crystal, which is in short and dense state. A mount of AlTi were observed at the interfacial layer near the Ti base metal while intermetallic compound like Al_3Ti, $TiSi_3$ were formed near the Al base metal, and the $Al_{11}Ti_5$ transition phase was found in the center of the interface layer due to the uneven distribution inside the weld pool during the welding process. Tensile test results show that the average tensile strength of joints is up to 182.6 MPa, *which is about* 97.6% *of aluminum base metal*. Fracture is prone to occur in the base metal with a certain amount of necking.

Key words: bypass-current MIG welding-brazed; dissimilar metals; joint characteristics; mechanical properties

Effect of rotational velocity of tool on mechanical properties of stationary shoulder friction stir welding JI Shude[1], MENG Xiangchen[1], HUANG Yongxian[1], GAO Shuangsheng[1], LU Hao[2], MA Lin[1] (1. Faculty of Aerospace Engineering, Shenyang Aerospace University, Shenyang 110136, China; 2. State Key Laboratory of Advanced Welding and Joining, Harbin Institute of Technology, Harbin 150001, China; 3. CSR Qingdao Sifang Locomotive and Rolling Stock Company, Limited, Qingdao 266111, China). pp 51 – 54

Abstract: Stationary shoulder friction stir welding (SSFSW) of 6005A-T6 aluminum alloy was investigated on basis of a self-designed stationary shoulder equipment. The results show that tensile strength and elongation of defect-free SSFSW joint with gloss surface both increase and then decrease with increasing rotational velocity of tool, and no cracks appear at the bending degree of 180°. At a constant welding speed of 200 mm/min and the rotational velocity of 1 800 r/min, the tensile strength of joint reaches the maximum value of 234 MPa and the

strength factor is 79%. The distribution of hardness of SSFSW joint presents W-shape and the minimum hardness appears in heat affected zone. The softening degree of joint increases with the increase of rotational velocity of tool. Fracture position of SSFSW occurs in thermo-mechanically affected zone and the fracture surface presents the typical ductile fracture.

Key words: stationary shoulder friction stir welding; mechanical properties; rotational velocity of tool; fracture

Effects of strain rate on stress corrosion cracking of X80 pipeline steel in ku'erle soil environment XIE Fei, WANG Dan, WU Ming, SUN Dongxu (College of Petroleum Engineering, Liaoning Shihua University, Fushun 113001, China). pp 55 – 58

Abstract: Slow strain rate testing (SSRT), potention dynamic polarization curves and scanning electron microscope (SEM) were employed to study the stress corrosion cracking (SCC) behavior of X80 pipeline steel in Ku'erle soil simulated solution. The results showed that the corrosion rate of X80 steel first increased and then decreased with the increase of strain rate. When the strain rate was 5×10^{-7}/s, the corrosion phenomenon of X80 steel was not obvious. At this time. electrochemical corrosion played a decisive role. When the strain rate was 5×10^{-6}/s, the corrosion behavior of X80 steel was the most serious. This is due to the combined effects of electrochemical and mechanical on the electrode surface, solution. which the mechanical action was dominating role

Key words: X80 pipeline steel; simulated soil solution; strain rate; stress corrosion cracking

Wettability of Sn-0.3Ag-0.7Cu-*x*Sb lead-free solders ZHANG Liang[1,2], TU K N[2], SUN Lei[1], GUO Yonghuan[1], HE Chengwen[1] (1. School of Mechanical and Electrical Engineering, Jiangsu Normal University, Xuzhou 221116, China; 2. Department of Materials Science and Engineering, University of California, Los Angeles 90095, USA). pp 59 – 62

Abstract: Effect of Sb on the wettability of Sn-0.3Ag-0.7Cu lead-free solders was investigated, with different atmospheres and fluxes, the wetting balance tester was used to analyze the wettability of Sn-0.3Ag-0.7Cu-*x*Sb solders. The results indicates that small amount of Sb can enhance the wettability of Sn-0.3Ag-0.7Cu solders. With the N_2 atmosphere, the wettability of Sn-0.3Ag-0.7Cu-*x*Sb can be increased obviously, which can be attributed to the resistance of oxidation (molten solder). Combing different fluxes, the wettability of lead-free solder can represent variation, the suitable flux can improve the wettability of Sn-0.3Ag-0.7Cu-*x*Sb solders.

Key words: lead-free solders; wettability; atmosphere; flux

Microstructure and mechanical properties of aluminum/stainless steel brazed joint with torch brazing YANG Jinlong[1], XUE Songbai[1], XUE Peng[1], DAI Wei[2], LÜ Zhaoping[1], ZHANG Man[3] (1. College of Materials Science and Technology, Nanjing University of Aeronautics and Astronautics, Nanjing 210016, China; 2. Zhejiang Xinrui Welding Material Company Limited, Shengzhou 312452, China; 3. College of Mechanical Engineering, Huaiyin Institute of Technology, Huaian 223003, China). pp 63 – 66

Abstract: The wettability, microstructure, intermetallic compound (IMC) layer and mechanical properties of aluminum/stainless steel joints brazed with Zn-*x*Al filler metals were investigated by means of scanning electron microscope, energy dispersive X-ray spectrometer and X-ray diffraction. The results indicate that the oxide film on the base metal could be effectively removed by the modified CsF-RbF-AlF_3 flux, and the excellent mechanical properties of the brazed joints were obtained. The spreading area as well as the clearance filling ability of Zn-*x*Al filler metal was both improved with by increasing the content of Al in the filler metals. However, the shear strength of the joint increased first and decreased afterwards, and the best mechanical property of brazed joint is obtained when the content of Al is 15%. It has been found that when the content of Al is low, the interfacial layer is composed of Zn-rich and Fe_4Al_{13} phase. As for the excessive amount of Al, additional Fe_2Al_5 phase is visible at the interface.

Key words: torch brazing; aluminum; stainless steel; microstructure; shear strength

Microstructure and properties of in-situ synthesized ceramic phase reinforced Fe-based coating by laser cladding QIAO Hong, LI Qingtang, FU Hanguang, LEI Yongping (School of Materials Science and Engineering, Beijing University of Technology, Beijing 100124, China). pp 67 – 69

Abstract: Laser cladding include Ti-Fe, B4C Fe-based alloy coating was fabricated on the surface of Cr12MoV automotive mold steel by using 6 kW fiber laser, in-situ synthesized TiC + TiB_2 ceramic phase reinforced Fe-based coating on the surface of Cr12MoV automotive mold steel. The gains are refined. Phases were presented in the coating evolved into TiB_2, TiC and α-Fe. Dese and defect-free coating with metallurgical joint to the substrate was obtained. Cladding layer 1.2 mm from the surface of the highest microhardness is up to 1 000 HV.

Key words: Fe-Cr-B alloy; laser cladding; in-situ synthesized; microhardness

Shear strength analysis of transverse fillet welds based on structural stress method NIE Chunge[1], WEI Hongliang[1], DONG Pingsha[2], ZHAO Wenzhong[1] (1. School of Traffic and Transportation Engineering, Dalian Jiaotong University, Dalian 116028, China; 2. School of Naval Architecture and Marine Engineering, University of Michigan, Ann Arbor 48109, USA). pp 70 – 74

Abstract: A structural stress based shear strength theory was established for transverse fillet welds in this paper, the new equations for calculating shear strength of fillet welds were provided, and some problems about shear strength of fillet welds were investigated. The results show that, theoretical failure angle of welds subjected unidirectional shear force is 22.5°, and both weld toe angle and load condition could also affect failure angle. In addition, the weld with 30° weld toe angle subjected unidirectional shear force possesses maximum load capacity, and the load